Plasmonic Enhancement of Raman Scattering from the Organic Solar Cell Material P3HT/PCBM by Triangular Silver Nanoprisms

ARTICLE *in* THE JOURNAL OF PHYSICAL CHEMISTRY C · OCTOBER 2011

Impact Factor: 4.77 · DOI: 10.1021/jp206853u

5 AUTHORS, INCLUDING:

Michael Salvador
Friedrich-Alexander-University of Erlangen-…

36 PUBLICATIONS **302** CITATIONS

SEE PROFILE

THE JOURNAL OF PHYSICAL CHEMISTRY C

ARTICLE

pubs.acs.org/JPCC

Plasmonic Enhancement of Raman Scattering from the Organic Solar Cell Material P3HT/PCBM by Triangular Silver Nanoprisms

Marina Stavytska-Barba,[†] Michael Salvador,[‡] Abhishek Kulkarni,[‡,§] David S. Ginger,[‡] and Anne Myers Kelley*[,†]

[†]School of Natural Sciences, University of California, Merced, 5200 North Lake Road, Merced, California 95343, United States

[‡]Department of Chemistry, University of Washington, Seattle, Washington 98195-1700, United States

Supporting Information

ABSTRACT: Resonance Raman spectra have been obtained for the organic solar cell blend poly(3-hexylthiophene)/[6,6]-phenyl C_{61}-butyric acid methyl ester (P3HT/PCBM) at excitation wavelengths ranging from 364 to 633 nm, in both the presence and absence of triangular Ag nanoprisms with varying plasmon resonance frequencies. For ~35 nm polymer films deposited over nanoprisms, the nanoprisms enhance the sample-averaged Raman scattering intensities by factors of 2−20 depending on wavelength and nanoprism density. The weak blend fluorescence is enhanced by approximately the same factor as the Raman scattering, implying negligible excited-state quenching by the metal. The Raman peak positions and relative intensities are unaffected by the nanoprisms, indicating negligible morphological or chemical changes to the P3HT. The observed Raman enhancements are qualitatively consistent with previously observed enhancements in charge-carrier (positive polaron) yields for P3HT/PCBM deposited over silver nanoprisms.

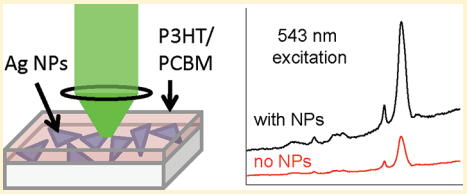

INTRODUCTION

Organic semiconductor blends based on the bulk heterojunction approach have been studied intensely as materials for photovoltaic devices.[1−4] These materials are attractive candidates for solar cells because they can be produced inexpensively in large quantities and deposited onto flexible substrates in a variety of sizes and shapes. The physical and optical properties of these materials can be varied by changing both the structures of the organic materials and the processing conditions. While organic photovoltaics with efficiencies exceeding 9% are now being reported, even the best conjugated polymer-based devices still fall short of crystalline silicon solar cells in performance. Factors limiting the performance of organic photovoltaics currently include the absorption of only part of the solar spectrum, carrier recombination losses following light absorption, and excess potential energy loss during the charge dissociation step. The long-term stability of organic materials also remains an issue for their use in outdoor applications.

There have been a number of recent reports that the conversion efficiencies of solar photovoltaic devices are, or might be, improved by incorporating plasmonically active metal nanostructures into the device.[5−28] For bulk heterojunction devices based on polymer/fullerene blends, power conversion efficiency enhancements of 15−70% have been reported through the use of metal nanoparticles.[8−11,13,14,27,28] (It should be noted, however, that some workers have reported no such enhancement[29,30] and other negative results may have gone unpublished.) Observed enhancements could have a number of causes, including indirect effects such as changes in the morphology of the material. Improved charge transport at the electrodes or through the material has also been suggested.[11,12,18,20,21,30] However, it appears likely that at least some of the reported effects have their origin in the electromagnetic properties specific to plasmonically active metals. These include increasing the fraction of the incoming light absorbed by the material[5−10,13−17,19,20,22−24,26−28] through near-field enhancement, scattering (path length enhancement), and/or waveguiding depending on the metallic nanostructure and device geometry,[26,31] as well as increasing the probability for exciton dissociation.[14,27]

Local enhancement of electromagnetic fields by plasmonically active nanostructures manifests itself in a number of other ways including the phenomenon of surface enhanced Raman scattering (SERS).[32−35] Standard electromagnetic SERS theory holds that the Raman scattering enhancement is simply the product of the enhancements of the local electromagnetic field intensities at the incident and Raman scattered wavelengths.[33,36] This simple relationship may be complicated by chemical enhancement from molecule−metal charge transfer,[37] the orientation of the Raman polarizability tensor relative to the metal surface, and effects of molecular electronic resonance.[38−40] Despite these caveats, the magnitude of the SERS enhancement should provide a reasonable measure of the electromagnetic field enhancement, and the SERS experiment can be carried out in an actual device structure or closely related geometries. In addition, any structural changes in the molecules nearest to the metal surface will be manifested as changes in the positions and/or relative intensities of the peaks in

Received: July 18, 2011
Revised: September 8, 2011
Published: September 15, 2011

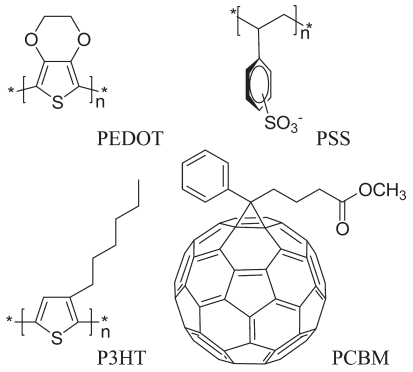

Figure 1. Structures of PEDOT, PSS, P3HT, and PCBM.

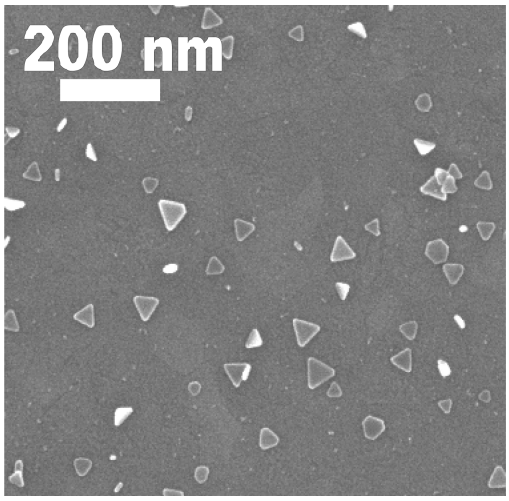

Figure 2. SEM of representative Ag nanoprisms.

the SERS spectrum compared to the unenhanced Raman spectrum. This structural sensitivity allows for examination of chemically specific effects of metal nanoparticles on the organic materials which would also be expected to affect the performance of photovoltaic cells.

We recently reported a SERS study of poly(3,4-ethylenedioxythiophene)−poly(styrenesulfonate) (PEDOT:PSS), a polymer blend often used as a hole collecting contact in organic solar cells[41] (Figure 1). Many of the device geometries reported to display power conversion efficiency enhancement have the metal nanoparticles in direct contact with PEDOT:PSS. In the doped (oxidized) form used, PEDOT:PSS is essentially transparent in the visible and increased light absorption should not be an available plasmonic enhancement mechanism. We observed SERS enhancement factors of about 2−30 depending on metal, excitation wavelength, and nanoparticle geometry. We also observed significant changes in the spectrum of the PEDOT component in the presence of metals, particularly Ag. These were interpreted to show that at low light intensities, silver nanoparticles promote the reoxidation of chemically reduced PEDOT and may therefore protect against the formation of nonconducting dedoped regions of PEDOT:PSS coated ITO.[42] However, at higher light intensities there was evidence for silver-induced photooxidation of PEDOT by addition of oxygen to the thiophene rings, disrupting the pi-conjugation.

Here we extend the SERS technique to films of poly(3-hexylthiophene)/[6,6]-phenyl C_{61}-butyric acid methyl ester (P3HT/PCBM, Figure 2), one of the best studied polymer blends used in bulk heterojunction organic polymer solar cells. Preliminary experiments utilized spherical nanoparticles similar to those used in our prior PEDOT:PSS study. However, we have chosen to focus on samples in which the polymer blend is deposited over triangular silver nanoprisms.[16,43−49] These nanoprisms have many desirable properties including large electromagnetic field enhancements particularly at the corners, broad tunability of their plasmon resonances across the visible spectrum, and self-assembly without aggregation onto silanized glass surfaces. Furthermore, direct spectroscopic evidence for enhanced charge-carrier generation has been demonstrated in this system.[16] Here we use the SERS enhancements as a measure of the extent of electromagnetic field enhancement caused by the nanoparticles and also to examine any changes in the Raman spectral characteristics that might indicate effects of the metal on the chemistry or morphology of the nearby organic material.

EXPERIMENTAL METHODS

Silver nanoprisms were synthesized via photoinduced conversion with pH control.[50,51] Figure 2 shows a representative SEM image. The nanoprisms were 11−12 nm thick with side lengths ranging from 27 to 40 nm; changing the length over this range shifts the plasmon resonance from about 440 to 550 nm. The nanoprisms were overcoated with a layer of 1:1 P3HT/PCBM having a thickness of about 35 nm. Self-assembly of the silver nanoprisms and polymer film processing were performed as described in ref 16.

Optical absorption spectra were obtained on a Cary 50 UV−vis spectrophotometer and an Agilent 8453 UV−vis diode array spectrometer. Nanoparticles were imaged on a field emission scanning electron microscope (FEI Sirion SEM).

Excitation for Raman spectroscopy was provided by either a Coherent Innova 90C-5 continuous wave argon-ion laser (363.8, 457.9, 488, and 514.5 nm) or helium−neon lasers (543.5, 612, and 632.8 nm). Spectra were obtained with a Jobin-Yvon T64000 Raman microscope system consisting of a 0.64 m triple spectrograph coupled to a confocal Raman microprobe based on an Olympus BX-41 microscope with an Olympus MPLFL100X objective (for visible excitation) or 40X UV objective (for near-UV excitation). The detector was a UV coated, back illuminated, liquid nitrogen cooled CCD with >50% quantum efficiency from 220 to 850 nm. Spectral resolution was better than 2 cm^{-1} for 632.8 nm excitation and about 4 cm^{-1} for 457.9 and 363.8 nm excitations. Excitation power at the sample was 0.2−0.3 mW, and the microscope stage was used to translate the sample along a line during data collection to average over the heterogeneous distribution of nanoprisms and to avoid heating or photochemical damage. Both the Raman and the fluorescence intensities of stationary samples exposed to air decayed rapidly with time, but scanning the samples under the excitation beam prevented this decay. The measured SERS intensities were linear with laser power from 0.08 to 0.24 mW, indicating negligible photodegradation.

For each sample and at each excitation wavelength, four to ten spectra with 60−360 s accumulation times were collected and averaged. The raw spectra were divided by the spectrum of a broad band light source to remove intensity fluctuations due to pixel-to-pixel sensitivity variations and etaloning of the CCD at longer wavelengths. Fluorescence backgrounds were removed

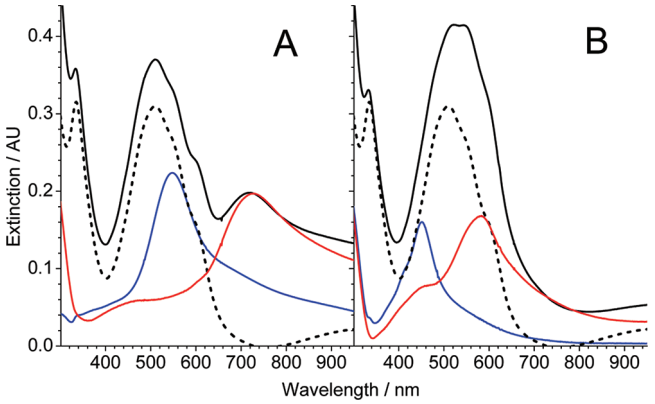

Figure 3. Measured extinction spectra for two samples containing different sized silver nanoprisms: black solid, NP with P3HT/PCBM; black dashed, P3HT/PCBM alone; blue, NP alone; red, modified NP extinction (NP with P3HT/PCBM minus P3HT/PCBM alone).

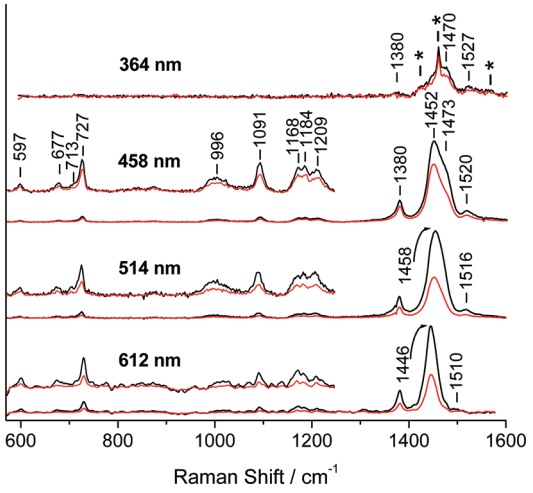

Figure 4. Raman spectra for the sample of Figure 3A at the indicated excitation wavelengths: red, P3HT/PCBM alone; black, P3HT/PCBM with NP. Vertical scaling and offsets for the different excitation wavelengths are arbitrary. All labeled peaks belong to P3HT. The asterisks mark the PCBM peaks at 1425, 1464, and 1573 cm^{-1}.

using Microcal Origin 6.0. The Raman spectra were calibrated in frequency by using the Raman bands of cyclohexane. Areas under Raman peaks were determined using the GRAMS/32 (Galactic Industries) curve fitting algorithm to fit mixed Gaussian−Lorentzian peak profiles.

The experimental SERS enhancement for each line at each excitation wavelength was calculated as the integrated area for the P3HT (or PCBM) peak in the presence of nanoparticles divided by that in the absence of nanoparticles after correcting for any differences in accumulation time. The theoretical SERS enhancement F, is given by standard electromagnetic theory as[36]

$$F \approx |E(\omega_{\mathrm{Laser}})/E_0(\omega_{\mathrm{Laser}})|^2 |E(\omega_{\mathrm{Scatt}})/E_0(\omega_{\mathrm{Scatt}})|^2 \qquad (1)$$

where $E_0(\omega)$ is the incident electric field at ω and $E(\omega)$ is the field in the presence of the metal. F depends on the position and orientation of the scattering molecule relative to the metal surface and to the polarizations of the incident and scattered photons. The expected frequency dependence of the enhancement

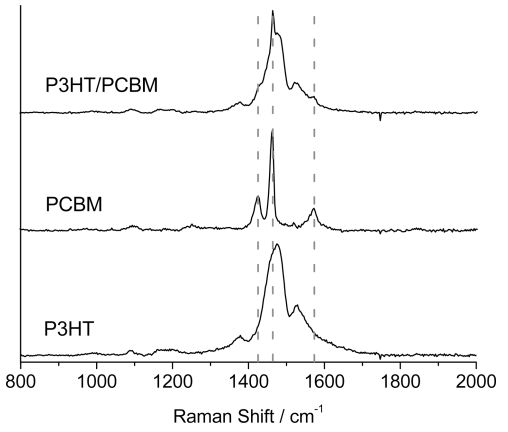

Figure 5. Raman spectra of a 1:1 blend of P3HT/PCBM, PCBM alone, and P3HT alone at 364 nm excitation in the absence of nanoparticles. Dashed lines indicate the positions of the three strongest PCBM lines.

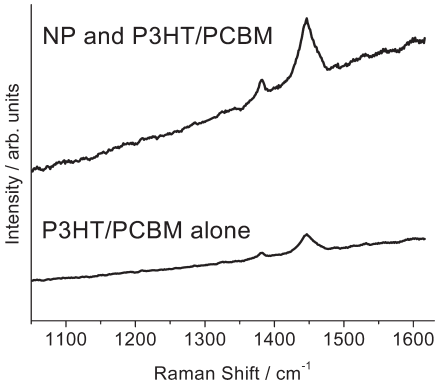

Figure 6. Total emission spectrum at 612 nm excitation for the sample in Figure 3B.

may be approximated as[36]

$$F = G^*A(\omega_{\mathrm{Laser}})A(\omega_{\mathrm{Scatt}}) + 1 \qquad (2)$$

where $A(\omega_{\mathrm{Laser}})$ and $A(\omega_{\mathrm{Scatt}})$ are the measured plasmon extinction profiles at the excitation and emission frequencies, respectively, and G is a scaling factor. We have added the factor of 1 to the enhancement profile as it is usually defined in order to obtain the physically correct result that F approaches unity far from any plasmon resonance.

RESULTS

Nine different silver nanoprism samples with plasmon resonance maxima from 440 to 548 nm were examined. When P3HT/PCBM was deposited on top of the nanoprisms, the plasmon resonances shifted to 552−735 nm. For example, the plasmon resonance of the nanoprisms shown in Figure 2 shifted from 492 to 674 nm with deposition of a P3HT/PCBM layer, while the resonances of smaller and larger nanoprisms shifted from 451 to 583 nm and from 548 to 727 nm, respectively (Figure 3). Modified extinction spectra of nanoprisms under the P3HT/PCBM layer were calculated by subtracting the P3HT/PCBM extinction spectra from the extinction spectra of P3HT/PCBM deposited on top of the silanized silver nanoprisms.

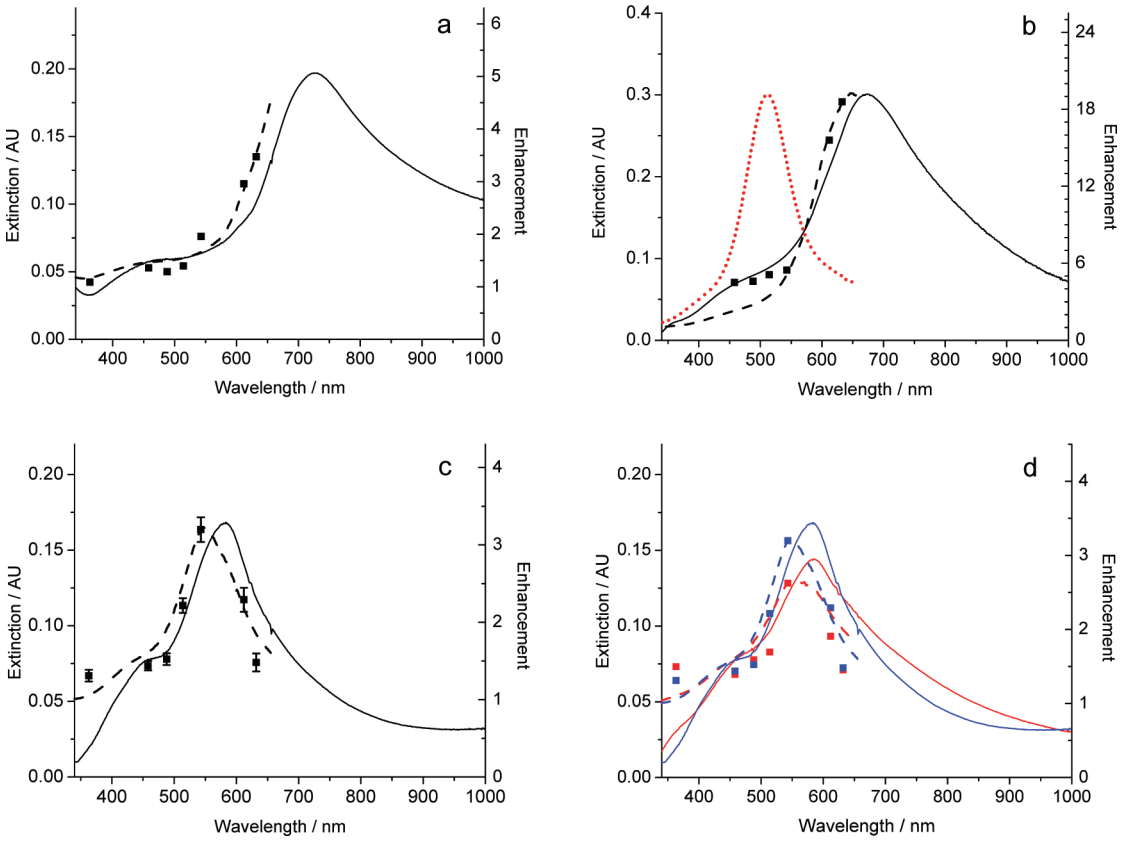

Figure 7. Experimental Raman enhancement factors for the ~1455 cm^{-1} P3HT band (points), modified NP extinction spectra (solid), and theoretical enhancements calculated from modified NP spectra using eq 2 (dashed). Estimated uncertainties in the experimental enhancements are shown for one data set (c). The red dashed curve in (b) is the theoretical enhancement calculated from the unmodified NP extinction spectrum. The blue and red curves in (d) compare two samples with similar extinction spectra.

Samples with different extinction maxima have different spectral overlaps with P3HT/PCBM.

Figure 4 shows Raman spectra of P3HT/PCBM alone (red) and of P3HT/PCBM deposited on top of silver nanoprisms (black) at four different excitation wavelengths. As expected from the modified extinction spectrum of the nanoprisms (red curve on Figure 3 left), enhancement of the Raman scattering is greatest at 612 nm and smallest for 364 nm excitation. Since P3HT absorbs much more strongly than PCBM in the visible, Raman bands of PCBM are observed only at 364 nm excitation (see Figure 5). Raman spectra at 364 nm are noisy because neither P3HT nor PCBM absorb strongly at 364 nm. Spectra excited at 612 and 633 nm (not shown in Figure 4) exhibit residual features, not completely removed by division by the broad band light source, from pixel-to-pixel sensitivity variations and etaloning of the CCD due to strong fluorescence of P3HT/PCBM at longer wavelengths. As shown in Figure 6, this fluorescence is enhanced by the same amount as the Raman scattering. Equal enhancement of the Raman and fluorescence components was observed in different samples having very different enhancement factors.

Detailed examination of the Raman spectra at 363.8, 457.9, 488, 514.5, 543.5, 612, and 632.8 nm excitation wavelengths shows that the frequencies of most Raman bands do not vary much with excitation wavelength. (The long-lived charge carriers absorb maximally at longer wavelengths[16,52,53] and are apparently not observed in these steady-state Raman spectra.) Two bands clearly do shift to higher frequencies with shorter excitation wavelength: the band at 1446 cm^{-1} with 612 nm excitation shifts to 1458 cm^{-1} at 514 nm and to 1470 cm^{-1} at 458 and 364 nm excitation, while the 1510 cm^{-1} band shifts to 1516 cm^{-1} at 514 nm, to 1520 cm^{-1} at 458 nm, and to 1527 cm^{-1} at 364 nm excitation. Both of these bands have large contributions from C═C thiophene ring in-phase stretching (see calculations in the Supporting Information). Shifting of the dominant conjugated stretching mode to lower frequency as the excitation is tuned to the red has been observed in a number of related conjugated polymers and oligomers and is attributed to preferential resonance with more planar structures having greater effective conjugation lengths.[41,54−56] The effect is particularly strong at 364 nm excitation, but this may have contributions both from preferential excitation of short conjugation length segments and from differing resonance conditions, as 364 nm overlaps both the first and second strongly allowed electronic transitions. There appear to be no variations in Raman frequencies at any excitation wavelength between samples with and without silver nanoprisms.

Figure 7 shows the modified nanoprism extinction spectra for some of the samples examined, experimental Raman enhancements, and theoretical enhancements. Figure 7b compares theoretical enhancements calculated using the extinction spectrum of the nanoprisms alone (measured before the P3HT/PCBM layer is deposited) and the modified extinction spectrum (nanoprisms with P3HT/PCBM minus P3HT/PCBM alone). The agreement between experimental and theoretical enhancements is

clearly much better when the modified extinction spectrum is used. Figure 7d compares two very similar samples which both have modified extinction maxima at 583 nm but different spectral band shapes. Even small changes in extinction spectra influence the experimental enhancements. The Raman enhancements displayed are calculated for the strongest line (the P3HT line ~1455 cm^{-1}), but all of the Raman bands appear to be enhanced by the same factor to within the accuracy of the measurements. This also applies to the PCBM bands at the UV excitation wavelengths where they have enough intensity to be detected.

DISCUSSION

The frequencies of the strongly Raman-active modes of P3HT do not appear to be changed by the presence of silver or gold nanoparticles. Additionally, there are no Raman bands that are reproducibly enhanced more than others by incorporation of metal nanoparticles. These two observations indicate that the metal causes no significant changes in either the ground-state structure or the nature of the resonant excited state. This result is in strong contrast to our previous results for PEDOT:PSS, where we found not only strong enhancement but also large changes in the appearance of the Raman spectra. Our results suggest that the interaction of P3HT with these metal nanoparticles is best characterized as purely electromagnetic, with a negligible chemical component.

The maximum experimental Raman enhancement factors range from about 2 to 20 for samples prepared with different NPs. This is very small compared with typical reported SERS enhancements in the 10^4 to 10^6 range or even higher. We believe that there are two principal reasons for the small measured enhancements. First, the NPs are, on average, spaced fairly far apart on the substrate; SEM images (see Figure 2) indicate that only a small fraction of the surface is covered with NPs. That, combined with the ~35 nm thickness of the polymer blend layer, means that most of the P3HT/PCBM in the sample is not close to a NP. Second, the presence of organic ligands on the NPs may prevent the polymer blend from closely approaching the metal surface. Indeed, TEM images (Figure S4, Supporting Information) suggest that the ligand shell on these prisms has a thickness of ~0.41 nm. The surface chemistry of the nanoprisms is not well-defined, but it is believed that they are capped with citrate and/or bis(*p*-sulfonatophenyl)-phenylphosphine ligands. The latter is a rather large ligand that may not be displaced by P3HT or PCBM.

These two issues were further explored by carrying out finite difference time domain (FDTD) simulations of the electric field within a rectangular slab of P3HT/PCBM (300 nm × 300 nm square, 35 nm thick) containing one NP (22 nm side length, 13 nm thick; see Supporting Information). The electromagnetic enhancement (approximated as $|E|^4$ at the plasmon resonance peak) averaged over the sample volume is approximately 5000 for bare NPs, still much smaller than typical SERS enhancements which can reach 10^6, but drops to about 60 when the NP is assumed to be covered by a 1.9 nm thick ligand shell. There are many uncertainties in these simulated enhancements: the actual density of NPs on the surface is poorly defined, the Raman-active chromophore may be farther from the metal surface than the apparent ligand shell thickness estimated from TEM, and the calculated plasmon resonance is much sharper than that observed experimentally, probably reflecting heterogeneity in the sizes and/or shapes of the NPs. However, the simulation results suggest that the low experimental enhancements are reasonable. Further details on the FDTD calculations are given in the Supporting Information.

The wavelength dependence of the measured Raman enhancement agrees reasonably well with that predicted by simple electromagnetic SERS theory using our best experimental estimate of the plasmon extinction spectrum in the presence of the analyte.[57] Plasmon resonances shift significantly when the dielectric properties of the surrounding medium are changed (the basis for ultrasensitive plasmon-based sensing techniques),[58] so for our analysis we need the spectrum of the nanoprisms coated with P3HT/PCBM. We have assumed that this "modified NP" plasmon spectrum is obtained by subtracting the extinction spectrum of P3HT/PCBM from the spectrum of the NPs coated with P3HT/PCBM. This is correct only if the interaction with the metal does not change the analyte's absorption spectrum. In fact, when the analyte and the nanoparticle have resonances in the same spectral region, it is expected that both spectra will be changed,[59,60] but as most of the organic material is quite far from the NPs (vide supra) and should have a nearly unperturbed spectrum, simply subtracting the pure P3HT/PCBM spectrum from the NP+P3HT/PCBM spectrum should give a good approximation to the modified NP plasmon spectrum.

Both Raman scattering and fluorescence can undergo electromagnetic enhancement near plasmonically active metal surfaces, but proximity to a metal surface also increases the nonradiative excited-state decay rate.[61,62] Studies of the distance dependence of SERS find that the SERS enhancement falls off very quickly with distance away from the metal surface, an order of magnitude over a distance of 2−3 nm.[33,58] Fluorescence, on the other hand, is generally quenched in close proximity to a metal surface but can be enhanced by plasmon resonance at longer distances.[63−65] When nearly all of the chromophores are adsorbed directly to the surface of the metal, the enhancement of the Raman signal is often accompanied by almost complete quenching of the fluorescence, allowing Raman spectra of highly fluorescent compounds such as laser dyes to be obtained with resonant excitation. Interestingly, we observe that the P3HT fluorescence is enhanced by almost exactly the same factor as the Raman scattering, as shown in Figure 6. Similar observations were made in other samples demonstrating a range of overall enhancement factors. This suggests that few of the P3HT chromophores are close enough to the metal surface to undergo quenching that is fast compared with the fluorescence lifetime in the absence of NPs. This result is consistent with the idea that the rather modest SERS enhancement may be attributed in part to bulky ligands capping the metal. The fluorescence enhancement presumably involves plasmonic enhancement of both the excitation rate and the radiative rate, and while it is possible that the latter could compete with charge separation in a device, this seems unlikely to be an important effect in view of the ultrafast rate of charge transfer at the heterojunction interface.

Kulkarni et al. have previously shown through photoinduced absorption spectroscopy that depositing P3HT/PCBM over silver nanoprisms increases the yield of polarons (charge carriers) by as much as a factor of 3.[16] This result was attributed to increased light absorption by the film in the presence of the plasmonically active nanoprisms. Although we are not working on the same samples as those and sample to sample variability is considerable, our results are qualitatively consistent with that work. The polaron yield should be linear with the incident light intensity so it should scale as $|E|^2$, while SERS scales as $|E|^4$. If we ignore the difference between the laser and scattered wavelengths,

then increased polaron yields of 1.2−3 (the range reported in ref 16) would be correlated to SERS enhancements of 1.4−9, which is roughly the range we observe (see Figure 7). The SERS experiments also give no evidence for any effect of the nanoprisms on the structure or morphology of the organic material, supporting a purely electromagnetic mechanism for the enhancements.

CONCLUSIONS

The resonance Raman and fluorescence spectra of P3HT/PCBM exhibit no obvious changes in the presence of silver nanoprisms beyond a modest enhancement in the overall intensity. The wavelength dependence of the enhancement agrees reasonably well with predictions based on the electromagnetic theory of SERS and the experimental plasmon spectra of the nanoprisms. Thus, in contrast to studies where the incorporation of nanoparticles or additives alters the polymer blend morphology,[66] the interaction of P3HT/PCBM with these silver nanoprisms appears to be characterized by enhancement of the local electromagnetic fields with no significant effects on the structure or morphology of the organic material.

ASSOCIATED CONTENT

Supporting Information. Density functional theory calculations (RB3LYP, 6-311 g(d,p)) of the ground-state structure and vibrational frequencies of a pentamer of 3-ethylthiophene and FDTD calculations of electromagnetic enhancement and TEM images of face-on stacks of nanoprisms, for measuring the thickness of ligand shells. This material is available free of charge via the Internet at http://pubs.acs.org.

AUTHOR INFORMATION

Corresponding Author

*E-mail amkelley@ucmerced.edu.

Present Addresses

§Boeing Research and Technology, Seattle, WA 98108.

ACKNOWLEDGMENT

Acknowledgment is made to the donors of the American Chemical Society Petroleum Research Fund for support of this research through Grant #48820-ND10 to A.M.K. D.S.G., A.P.K., and M.S. acknowledge support for the nanoprism/polymer sample preparation under the DOE Solar America Initiative N00014-08-1-1227.

REFERENCES

(1) Giridharagopal, R.; Ginger, D. S. *J. Phys. Chem. Lett.* **2010**, *1*, 1160–1169.
(2) Brabec, C. J.; Gowrisanker, S.; Halls, J. J. M.; Laird, D.; Jia, S.; Williams, S. P. *Adv. Mater.* **2010**, *22*, 3839–3856.
(3) Chen, L.-M.; Hong, Z.; Li, G.; Yang, Y. *Adv. Mater.* **2009**, *21*, 1434–1449.
(4) Gnes, S.; Neugebauer, H.; Sariciftci, N. S. *Chem. Rev.* **2007**, *107*, 1324–1338.
(5) Nah, Y.-C.; Kim, S.-S.; Park, J.-H.; Park, H.-J.; Jo, J.; Kim, D.-Y. *Electrochem. Commun.* **2007**, *9*, 1542–1546.
(6) Tvingstedt, K.; Persson, N.-K.; Inganas, O.; Rahachou, A.; Zozoulenko, I. V. *Appl. Phys. Lett.* **2007**, *91*, 113514.
(7) Sue, C.-W.; Hsieh, H.-T.; Su, G.-D. J. *Proc. SPIE* **2007**, *6656*, 66561L.
(8) Chang, Y. C.; Chou, F. Y.; Yeh, P. H.; Chen, H. W.; Chang, S.-H.; Lan, Y. C.; Guo, T. F.; Tsai, T. C.; Lee, C. T. *J. Vac. Sci. Technol., B* **2007**, *25*, 1899–1902.
(9) Kim, S.-S.; Na, S.-I.; Jo, J.; Kim, D.-Y.; Nah, Y.-C. *Appl. Phys. Lett.* **2008**, *93*, 073307.
(10) Chen, X.; Zhao, C.; Rothberg, L.; Ng, M.-K. *Appl. Phys. Lett.* **2008**, *93*, 123302.
(11) Naidu, B. V. K.; Park, J. S.; Kim, S. C.; Park, S.-M.; Lee, E.-J.; Yoon, K.-J.; Lee, S. J.; Lee, J. W.; Gal, Y.-S.; Jin, S.-H. *Sol. Energy Mater. Sol. Cells* **2008**, *92*, 397–401.
(12) Tong, S. W.; Zhang, C. F.; Jiang, C. Y.; Liu, G.; Ling, Q. D.; Kang, E. T.; Chan, D. S. H.; Zhu, C. *Chem. Phys. Lett.* **2008**, *453*, 73–76.
(13) Morfa, A. J.; Rowlen, K. L.; Reilly, T. H., III; Romero, M. J.; van de Lagemaat, J. *Appl. Phys. Lett.* **2008**, *92*, 013504.
(14) Chen, F.-C.; Wu, J.-L.; Lee, C.-L.; Hong, Y.; Kuo, C.-H.; Huang, M. H. *Appl. Phys. Lett.* **2009**, *95*, 013305.
(15) Yoon, W.-J.; Jung, K.-Y.; Liu, J.; Duraisamy, T.; Revur, R.; Teixeira, F. L.; Sengupta, S.; Berger, P. R. *Sol. Energy Mater. Sol. Cells* **2010**, *94*, 128–132.
(16) Kulkarni, A. P.; Noone, K. M.; Munechika, K.; Guyer, S. R.; Ginger, D. S. *Nano Lett.* **2010**, *10*, 1501–1505.
(17) Rand, B. P.; Peumans, P.; Forrest, S. R. *J. Appl. Phys.* **2004**, *96*, 7519–7526.
(18) Barazzouk, S.; Hotchandani, S. *J. Appl. Phys.* **2004**, *96*, 7744–7746.
(19) Heidel, T. D.; Mapel, J. K.; Singh, M.; Celebi, K.; Baldo, M. A. *Appl. Phys. Lett.* **2007**, *91*, 093506.
(20) Pan, S.; Rothberg, L. J. *Proc. SPIE* **2007**, *6641*, 664109.
(21) Park, J.-W.; Ullah, M. H.; Park, S. S.; Ha, C.-S. *J. Mater. Sci.: Mater. Electron.* **2007**, *18*, S393–S397.
(22) Hägglund, C.; Zach, M.; Kasemo, B. *Appl. Phys. Lett.* **2008**, *92*, 013113.
(23) Yang, M. D.; Liu, Y. K.; Shen, J. L.; Wu, C. H.; Lin, C. A.; Chang, W. H.; Wang, H. H.; Yeh, H. I.; Chan, W. H.; Parak, W. J. *Opt. Express* **2008**, *16*, 15754–15758.
(24) Standridge, S. D.; Schatz, G. C.; Hupp, J. T. *J. Am. Chem. Soc.* **2009**, *131*, 8407–8409.
(25) Bai, W.; Gan, Q.; Song, G.; Chen, L.; Kafafi, Z.; Bartoli, F. *Opt. Express* **2010**, *18*, A620–A630.
(26) Tsai, S.-J.; Ballarotto, M.; Romero, D. B.; Herman, W. N.; Kan, H.-C.; Phaneuf, R. J. *Opt. Express* **2010**, *18*, A528–A535.
(27) Wu, J.-L.; Chen, F.-C.; Hsiao, Y.-S.; Chien, F.-C.; Chen, P.; Kuo, C.-H.; Huang, M. H.; Hsu, C.-S. *ACS Nano* **2011**, *5*, 959–967.
(28) Wang, D. H.; Kim, D. Y.; Choi, K. W.; Seo, J. H.; Im, S. H.; Park, J. K.; Park, O. O.; Heeger, A. J. *Angew. Chem., Int. Ed.* **2011**, 50.
(29) Topp, K.; Borchert, H.; Johnen, F.; Tunc, A. V.; Knipper, M.; von Hauff, E.; Parisi, J.; Al-Shamery, K. *J. Phys. Chem. A* **2010**, *114*, 3981–3989.
(30) Xue, M.; Li, L.; Tremolet de Villers, B. J.; Shen, H.; Zhu, J.; Yu, Z.; Stieg, A. Z.; Pei, Q.; Schwartz, B. J.; Wang, K. L. *Appl. Phys. Lett.* **2011**, *98*, 253302.
(31) Atwater, H. A.; Polman, A. *Nat. Mater.* **2010**, *9*, 205–213.
(32) Tian, Z.-Q.; Ren, B.; Wu, D.-Y. *J. Phys. Chem. B* **2002**, *106*, 9463–9483.
(33) Stiles, P. L.; Dieringer, J. A.; Shah, N. C.; Van Duyne, R. P. *Annu. Rev. Anal. Chem.* **2008**, *1*, 601–626.
(34) Kneipp, J.; Kneipp, H.; Kneipp, K. *Chem. Soc. Rev.* **2008**, *37*, 1052–1060.
(35) Lee, S. J.; Guan, Z.; Xu, H.; Moskovits, M. *J. Phys. Chem. C* **2007**, *111*, 17985–17988.
(36) Le Ru, E. C.; Grand, J.; Félidj, N.; Aubard, J.; Lévi, G.; Hohenau, A.; Krenn, J. R.; Blackie, E.; Etchegoin, P. G. *J. Phys. Chem. C* **2008**, *112*, 8117–8121.
(37) Kambhampati, P.; Child, C. M.; Foster, M. C.; Campion, A. *J. Chem. Phys.* **1998**, *108*, 5013–5026.
(38) Zhao, J.; Dieringer, J. A.; Zhang, X.; Schatz, G. C.; Van Duyne, R. P. *J. Phys. Chem. C* **2008**, *112*, 19302–19310.
(39) Zhao, J.; Jensen, L.; Sung, J.; Zou, S.; Schatz, G. C.; Van Duyne, R. P. *J. Am. Chem. Soc.* **2007**, *129*, 7647–7656.

(40) Kelley, A. M. *J. Chem. Phys.* **2008**, *128*, 224702.
(41) Stavytska-Barba, M.; Kelley, A. M. *J. Phys. Chem. C* **2010**, *114*, 6822–6830.
(42) Kim, J.-S.; Ho, P. K. H.; Murphy, C. E.; Baynes, N.; Friend, R. H. *Adv. Mater.* **2002**, *14*, 206–209.
(43) Munechika, K.; Chen, Y.; Tillack, A. F.; Kulkarni, A. P.; Plante, I. J.-L.; Munro, A. M.; Ginger, D. S. *Nano Lett.* **2010**, *10*, 2598–2603.
(44) Munechika, K.; Smith, J. M.; Chen, Y.; Ginger, D. S. *J. Phys. Chem. C* **2007**, *111*, 18906–18911.
(45) Sherry, L. J.; Jin, R.; Mirkin, C. A.; Schatz, G. C.; Van Duyne, R. P. *Nano Lett.* **2006**, *6*, 2060–2065.
(46) Murray, W. A.; Suckling, J. R.; Barnes, W. L. *Nano Lett.* **2006**, *6*, 1772–1777.
(47) Metraux, G. S.; Mirkin, C. A. *Adv. Mater.* **2005**, *17*, 412–415.
(48) Sun, Y.; Mayers, B.; Xia, Y. *Nano Lett.* **2003**, *3*, 675–679.
(49) Haes, A. J.; Van Duyne, R. P. *J. Am. Chem. Soc.* **2002**, *124*, 10596–10604.
(50) Jin, R.; Cao, Y. C.; Hao, E.; Metraux, G. S.; Schatz, G. C.; Mirkin, C. A. *Nature* **2003**, *425*, 487–490.
(51) Xue, C.; Mirkin, C. A. *Angew. Chem., Int. Ed.* **2007**, *46*, 2036–2038.
(52) Guo, J.; Ohkita, H.; Benten, H.; Ito, S. *J. Am. Chem. Soc.* **2010**, *132*, 6154–6164.
(53) Piris, J.; Dykstra, T. E.; Bakulin, A. A.; van Loosdrecht, P. H. M.; Knulst, W.; Trinh, M. T.; Schins, J. M.; Siebbeles, L. D. A. *J. Phys. Chem. C* **2009**, *113*, 14500–14506.
(54) Tran-Van, F.; Garreau, S.; Louarn, G.; Froyer, G.; Chevrot, C. *Synth. Met.* **2001**, *119*, 381–382.
(55) Gao, Y.; Grey, J. K. *J. Am. Chem. Soc.* **2009**, *131*, 9654–9662.
(56) Sakamoto, A.; Furukawa, Y.; Tasumi, M. *J. Phys. Chem.* **1992**, *96*, 1490–1494.
(57) McFarland, A. D.; Young, M. A.; Dieringer, J. A.; Van Duyne, R. P. *J. Phys. Chem. B* **2005**, *109*, 11279–11285.
(58) Willets, K. A.; Van Duyne, R. P. *Annu. Rev. Phys. Chem.* **2007**, *58*, 267–297.
(59) Haes, A. J.; Zou, S.; Zhao, J.; Schatz, G. C.; Van Duyne, R. P. *J. Am. Chem. Soc.* **2006**, *128*, 10905–10914.
(60) Kelley, A. M. *Nano Lett.* **2007**, *7*, 3235–3240.
(61) Galloway, C. M.; Etchegoin, P. G.; Le Ru, E. C. *Phys. Rev. Lett.* **2009**, *103*, 063003.
(62) Johansson, P.; Xu, H.; Käll, M. *Phys. Rev. B* **2005**, *72*, 035427.
(63) Tam, F.; Goodrich, G. P.; Johnson, B. R.; Halas, N. J. *Nano Lett.* **2007**, *7*, 496–501.
(64) Knobloch, H.; Brunner, H.; Leitner, A.; Aussenegg, F.; Knoll, W. *J. Chem. Phys.* **1993**, *98*, 10093–10095.
(65) Anger, P.; Bharadwaj, P.; Novotny, L. *Phys. Rev. Lett.* **2006**, *96*, 113002.
(66) Peet, J.; Kim, J. Y.; Coates, N. E.; Ma, W. L.; Moses, D.; Heeger, A. J.; Bazan, G. C. *Nat. Mater.* **2007**, *6*, 497–500.